ELSEVIER

Journal of Nuclear Materials 244 (1997) 44–50

journal of nuclear materials

Study of power load on TdeV divertor plates with an infrared camera

W. Zhang [a,b,*], T. Fall [a,b], B. Terreault [a,b], J. Gunn [a,b], J. Mailloux [a,b], A. Sarkissian [a,b], N. Richard [a,c]

[a] *Centre Canadien de Fusion Magnétique, 1804 Montée Ste-Julie, Varennes, Que., Canada J3X 1S1*
[b] *INRS-Énergie and Materiaux, Université du Québec, Varennes, Que., Canada*
[c] *MPB Techologies Inc., Dorval, Que., Canada*

Received 10 July 1996; accepted 4 November 1996

Abstract

An infrared (IR) camera has been installed on TdeV (Tokamak de Varennes) to view both the inner and the outer divertor plates. With a finite element code (PDE Protran), the energy deposited on the plates is calculated from the surface temperature profile measured by the IR camera. The experimental results have revealed that the divertor plate temperature decreases with an increase of the main plasma density, suggesting that the plasma detaches from the divertor plates at higher plasma densities (above 4.0×10^{19} m^{-3}). During divertor biasing, the heat flux increases on the plates of the 'active' divertor as a result of the $\boldsymbol{E} \times \boldsymbol{B}$ flow. However, energy deposition can be reduced by increasing the plasma density. The neutral gas pressure in the divertor region increases strongly at higher plasma density, and appears to be correlated with the reduction in deposited energy.

1. Introduction

Reducing the power flux deposition on the divertor plates is a major issue for the next generation of tokamak devices, such as ITER (international thermonuclear experimental reactor). According to the present ITER design, the peak power flux on the divertor plate would be around 20 MW/m^2, which is too high compared with the tolerable engineering limit of 5 MW/m^2. The excessive heat loads on the divertor plates will cause concern from both standpoints of mechanical integrity and erosion rate. Many efforts have been made to find a 'physics' solution for the reduction of the energy flux on the divertor plates. New operating regimes such as the 'radiative divertor' and 'divertor plasma detachment', in which the power flowing into the divertor region is distributed by radiation and charge exchange neutrals over large areas of the divertor, have been discovered [1–5]. These new divertor operating regimes may become the solution for reactor grade tokamak operation, although the detailed physical mechanisms involved require further investigation.

At TdeV (Tokamak de Varennes), experiments have been carried out to study the divertor characteristics under various discharge conditions. These include ohmic heating, divertor biasing, and lower hybrid (LH) current drive and heating discharges. It has been demonstrated [6,7] that divertor performance can be influenced by the application of an electric field in the scrape-off layer (SOL) via divertor plate biasing. During biasing, the impurity concentration is reduced, plasma rotation is affected in a controlled manner and divertor retention is significantly improved, opening the way to enhanced He-ash removal and radiative heat removal in the divertor [8–13]. Recent experimental studies also show that the beneficial effects of divertor biasing remain effective in the presence of lower hybrid (LH) current drive and heating [14]. These features make divertor biasing a potential technique to control the divertor performance in future tokamaks. However, during biasing, the radial electric field in the SOL region causes an $\boldsymbol{E} \times \boldsymbol{B}$ flow which drives the plasma particles directly onto the divertor plates. This may result in additional energy deposition on the surface of the plates.

* Corresponding author. Present address: JET Joint Undertaking, Abingdon, Oxfordshire, OX14 3EA, UK.

PII S0022-3115(96)00725-8

In this paper, the energy deposition on the TdeV divertor plates under various discharge conditions will be investigated. An infrared (IR) camera was installed to measure the surface temperature on both the inner and the outer divertor plates during the discharges. The paper is organized as follows. The discharge conditions and diagnostic instruments are described in Section 2. The calculation of energy deposition is presented in Section 3. Some experimental results during normal ohmic heating, divertor biasing and LH current drive/heating discharges are discussed in Section 4. A summary is given in Section 5.

2. TdeV and IR diagnostic

TdeV has a major radius $R = 0.87$ m and a minor radius $a = 0.27$ m. It can be operated in either an upper single-null divertor configuration or a double-null divertor configuration with plasma current and toroidal field limited to $I_p = 300$ kA and $B_T = 1.9$ T. The machine is equipped with biasable divertor plates [6,15] and lower hybrid current drive and heating capabilities [16]. To study the energy deposition on the divertor plates during various tokamak discharge conditions, an infrared (IR) camera has been installed on TdeV. Fig. 1 shows a schematic of the IR imaging system on TdeV. It consists of the IR camera

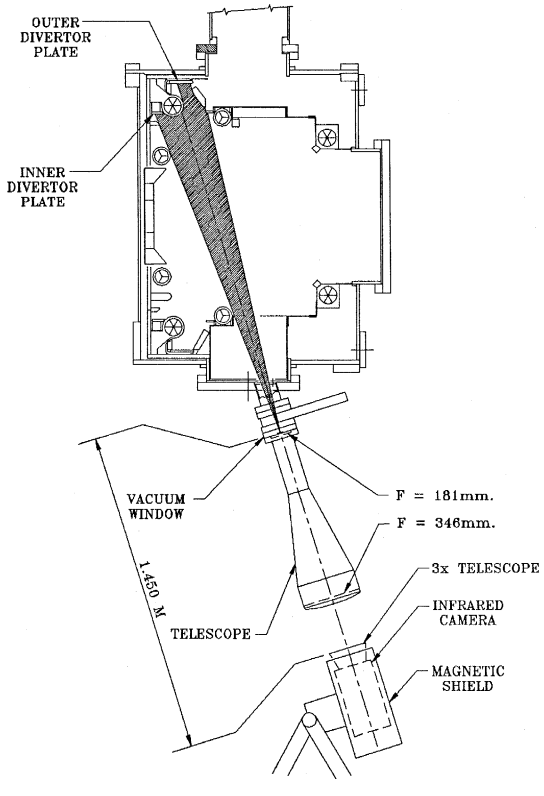

Fig. 1. Experimental set-up for infrared imaging of the divertor plates.

(Inframetrics 600 sensitive to radiation in the 3–5 μm range) with a 3× telescope, an optical telescope and a sapphire vacuum window of 50 mm diameter. The diagnostic setup is fairly straightforward. The camera is kept 1.45 m away from the tokamak to avoid magnetic field interference with its mechanical scanner. This severely limits the field of view of the camera due to the small aperture of the window. An optical telescope is required to improve the field of view for the IR camera. The telescope consists of two silicon lenses and is mounted directly on the sapphire window. This telescope optically projects the window to the position where the entrance pupil of the 3× telescope–camera system is located, and thus increases the field of view of the IR camera. Ray tracing calculations have shown that the telescope is able to provide a good field depth (±64 mm) and a spatial resolution of 1 mm on the divertor plates (overall spatial resolution of the system is about 2.5 mm). With this telescope, the IR camera is able to view an area of 240 cm × 180 cm in the object plane and covers a toroidal section of both inner and outer divertor plates.

Other diagnostics for measuring the divertor parameters include flush mounted Langmuir probes [17], thermocouples [18], ionization gauges and a bolometer array [19]. The Langmuir probes are used to measure the electron density and temperature in front of the plate. The thermocouples are used to measure temperature at a few locations in the plate. The ionization gauges are used to monitor the neutral gas pressure in the divertor chamber and the bolometry array is used to measure radiation losses from both main plasma and divertor plasma.

3. Calculation of the energy deposition on the divertor plates

The output from the IR camera consists of a standard RS170 video signal (60 fields/s, 262.5 line/field). The signal level of each pixel is a function of the local surface temperature. The calibration factor of the IR system is obtained by comparing the IR results with those of thermocouples which are embedded beneath the divertor plate. The video output of the camera is stored on video tape during tokamak discharges and digitized later for data processing. A radial profile of the surface temperature of the outer divertor plate is shown in Fig. 2 as a function of time during the discharge. This time evolution of the temperature can be used as a boundary condition to calculate the heat flux deposition on the divertor plate during the discharge.

The typical duration of TdeV discharges is over one second which is longer than the temperature equalization time over the finite thickness of the plate ($\tau = d^2/(2k/\rho c_p) \approx 0.67$ s, where $d = 8$ mm is the plate thickness, $k = 76$ W m^{-1} °C^{-1} is the thermal conductivity of graphite, $\rho = 1820$ kg m^{-3} is the mass density and $c_p =$

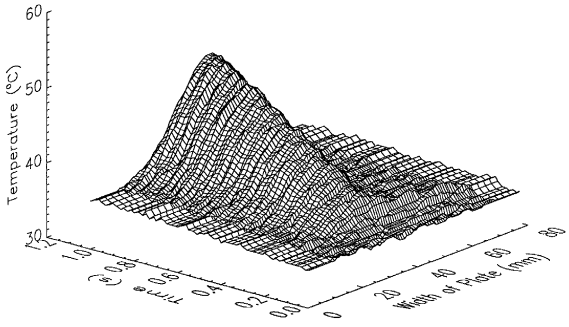

Fig. 2. A horizontal linescan of the infrared image (temperature versus distance along the width of the outer plate) is plotted against discharge time.

880 J kg^{-1} $°C^{-1}$ is the specific heat). The widely used semi-infinite one dimensional model [20–22] for heat flow is therefore not suitable for the pulse length of TdeV. A finite element analysis code (PDE/Protran code) [23,24] has to be employed to calculate the heat flux at the surface of the plate (the results calculated by the semi-infinite one dimensional model is 50% smaller than those calculated by the PDE/Protran code). The PDE/Protran code takes the measured surface temperature profile (Fig. 2) of the plates as the boundary condition and solves the heat conduction equation

$$\rho c_p \frac{\partial T}{\partial t} = \frac{\partial F_x}{\partial x} + \frac{\partial F_y}{\partial y} + \frac{\partial F_z}{\partial z} \quad (1)$$

over the cross-section of the divertor plate. Here T is the temperature, F is the heat flux in W/m^2. F_x, F_y, F_z are three components of the heat flux on the divertor plate, with F_z in the toroidal direction, F_x in the direction of major radius R, and F_y in the downward direction. ($\partial F/\partial z = 0$ due to toroidal symmetry of the heat flux distribution.) The heat loss of the plates on the time scale of one second is negligibly small because of the relatively poor contact with the copper backing. This has been checked with the thermocouple measurements [18]. The output of the code is a tabulation of the temperature and heat flux for preselected mesh nodes of cross section of the plate for different times during the discharge. Fig. 3(a), (b) show the radial profile of the temperature of the outer divertor plate and the radial heat flux distribution on the surface of the plate, respectively. Fig. 3(c), (d) show the power and energy deposition on the plate. They are obtained by integrating the heat flux over the entire surface area (power) and then integrating over the duration of the discharge (energy). Fig. 4 shows the energy deposition measured by both the IR system and the thermocouples, as a function of line averaged plasma density. The energy deposition measured by the thermocouple can be deduced from $E = \rho c_p V \Delta T$, where V is the volume of the divertor plates, $\Delta T = T_E - T_0$, T_0 is the initial temperature measured before the discharge and T_E is the equilibrium temperature of the plate. (The equilibration time is ~ 14 s; this is defined as the time when all the thermocouples under a plate reach the same value.) A total of 64 thermocouples were installed at different toroidal locations. They were used to measure the temperature of the divertor plates, secondary limiters and other components exposed

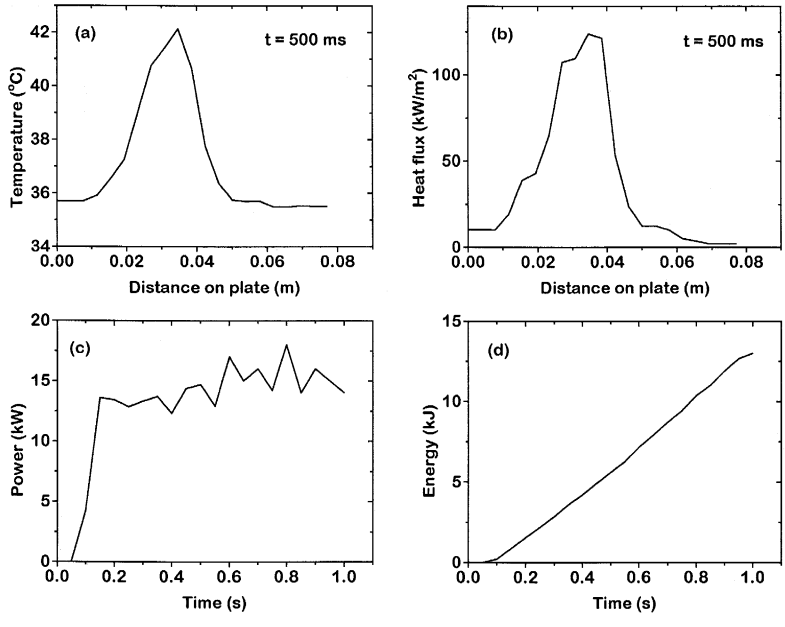

Fig. 3. Power deposition on the divertor plate calculated by PDE/Protran code. (a) Surface temperature profile. (b) Heat flux profile. (c) Total power deposition on outer plates. (d) Energy deposition during one second of discharge.

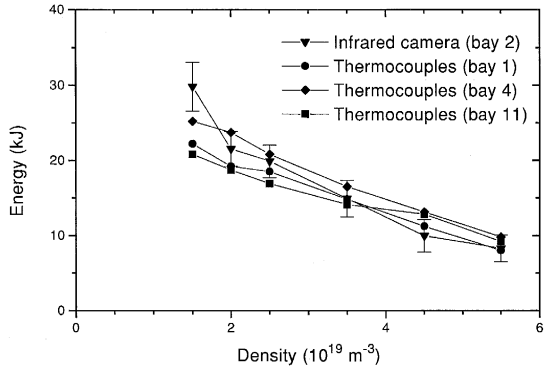

Fig. 4. Energy deposition measured by the IR camera and the thermocouples, as a function of the plasma line-average density.

to the plasma bombardment. The results of thermocouples shown in Fig. 4 were made on the inner plates at different toroidal locations specified by bay number. (There are 16 bays on TdeV.) The difference among the results of thermocouples and the IR camera may be due to the toroidal asymmetry in the energy deposition at different bays. This asymmetry becomes more severe when lower hybrid heating is applied. The cause of this phenomenon is currently under investigation.

4. Results and discussion

The data presented in the following were obtained during tokamak operations with an upper single null divertor configuration and standard discharge conditions of $B_T = 1.5$ T, $I_p = 190$ kA. The ion grad-B drift direction was pointing away from the X-point. The IR results of the power deposition on the divertor plates obtained during ohmic heating discharges, divertor biasing and lower hybrid current drive and heating will be discussed in Sections 4.1, 4.2 and 4.3.

4.1. Ohmic heating discharges

A density scan was performed during a series of normal ohmic heating discharges. The plasma density varied from 2×10^{19} m^{-3} to 7×10^{19} m^{-3} on a shot-to-shot basis. It is observed that the power flowing towards the divertor plate is reduced at higher plasma densities. Based on the surface temperature measurement of the divertor plate, the heat flux deposition is calculated and is shown in Fig. 5 for different plasma densities. The calculation shows that the heat flux decreases on the divertor plates at higher plasma densities, while bolometric measurements of the plasma radiation [19] show that the radiated power decreases in front of the divertor plate and increases towards the magnetic X-point. This indicates the formation of an intense radiative zone near the X-point. These results suggest the detachment of plasma from the divertor plates at higher plasma densities. The detached divertor has been observed in several tokamaks [1–4]. A general characteristic of the detached divertor operation is a strong pressure gradient in the scrape-off layer (SOL) from the midplane to the divertor plates. This can be achieved when sufficient neutral gas particles are present in the divertor region and the local temperature is low enough for charge exchange to dominant over ionization. Parallel momentum is removed from the plasma flowing to the target through charge exchange and elastic ion–neutral collisions [25]. Fig. 6(a) shows the electron density in the divertor as a function of the line averaged plasma density. The electron density in the divertor region was measured with the flush-mounted Langmuir probes [17]. The electron density in the divertor initially increases as the plasma density increases. However, above $\bar{n}_e = 4.0 \times 10^{19}$ m^{-3}, the divertor density starts to decrease. Fig. 6(b) shows that the electron temperature also decreases when the plasma density increases and reaches a value near 5 eV at plasma densities greater than 5×10^{19} m^{-3}. This is a signature of plasma detachment from the divertor plates. Fig. 6(c) shows the neutral gas pressure in the divertor region measured by the ionization gauge. The neutral pressure continuously increases as the main plasma density increases. This increase, along with the accompanying decreases in divertor plate density (when T_e drops to 5 eV), is consistent with detachment of the divertor plasma from the target plates.

4.2. Divertor biasing

One of the experimental programs in TdeV is divertor plate biasing with respect to the vacuum vessel and liner [6,15]. Biasing polarizes the whole central plasma via the good electrical connection of the SOL with the divertor plates along the separatrix. A radial electric field is established in the SOL between the separatrix and the first poloidal flux surface in contact with ground. The plasma flow in the SOL region is therefore influenced through the $\boldsymbol{E} \times \boldsymbol{B}$ drift and the transverse flow due to the $\boldsymbol{J} \times \boldsymbol{B}$ force. The charged particles of both polarities move in a

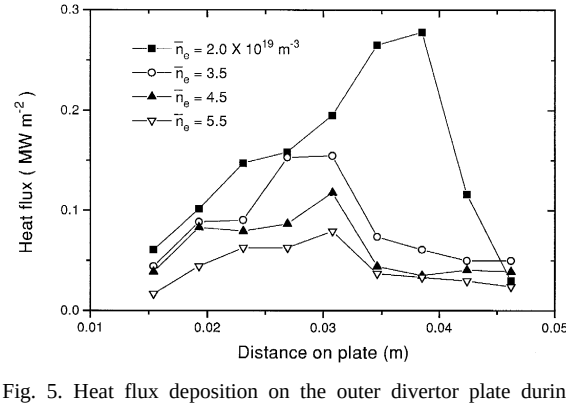

Fig. 5. Heat flux deposition on the outer divertor plate during normal plasma discharge at different plasma density.

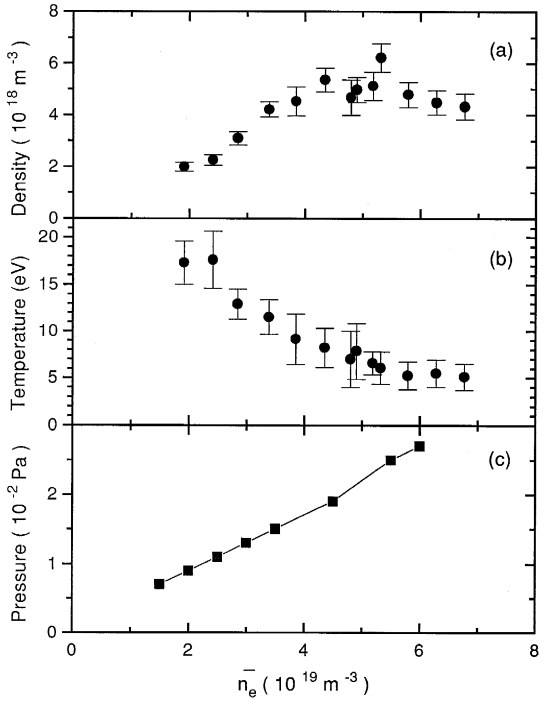

Fig. 6. Divertor parameters during an ohmic discharge. (a) Divertor electron density versus plasma density. (b) Divertor electron temperature versus plasma density. (c) Divertor neutral pressure versus plasma density.

poloidal direction toward the inner or outer divertor plate of the upper single null divertor depending on the bias polarity, and change the SOL and divertor plasmas. The influence of divertor biasing on the plasma parameters has been previously reported [8–13]. Biasing of the divertor plates leads to the enhancement of the divertor pumping efficiency and impurity retention. Biasing also changes the plasma poloidal rotation speed and the density gradient in the SOL [26] and reduces the turbulence level in the plasma [11]. However, it was recently found through infrared imaging that the heat flux increases on the divertor plates as a result of the $\boldsymbol{E} \times \boldsymbol{B}$ flow.

In the present experiments, the upper outer divertor plates were connected to the biasing power supply, while all the other plates were isolated from ground. The outer divertor plates could be biased in the range of -150 V to $+150$ V with respect to the tokamak chamber. The heat flux distribution changes drastically compared with a normal ohmic discharge. Most of the heat flux in this case was directed towards the outer divertor plates, which causes a substantial temperature increase on these plates. The heat flux deposited on the divertor plates has been computed. Fig. 7 shows the heat flux deposition on the divertor plates as a function of the biasing voltage for both the outer and the inner plates. The heat flux deposited on the outer plate increases as the negative biasing voltage increases. Positive divertor biasing has an equalizing effect on the heat flux distribution on the plates. The results are in agreement with recent theoretical study [27] which suggests that the divertor plate power load can be equalized by means of biasing. During the negative biasing phase, the neutral pressure also increases (Fig. 8(a)) due to increased particle flux to the divertor [28]. However, because the increase in

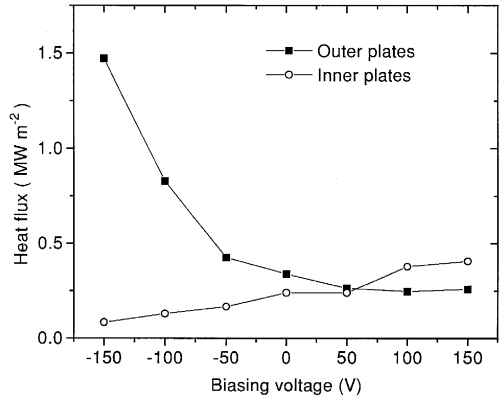

Fig. 7. Heat flux deposition on divertor plate as a function of the biasing voltage for both the outer and the inner plates.

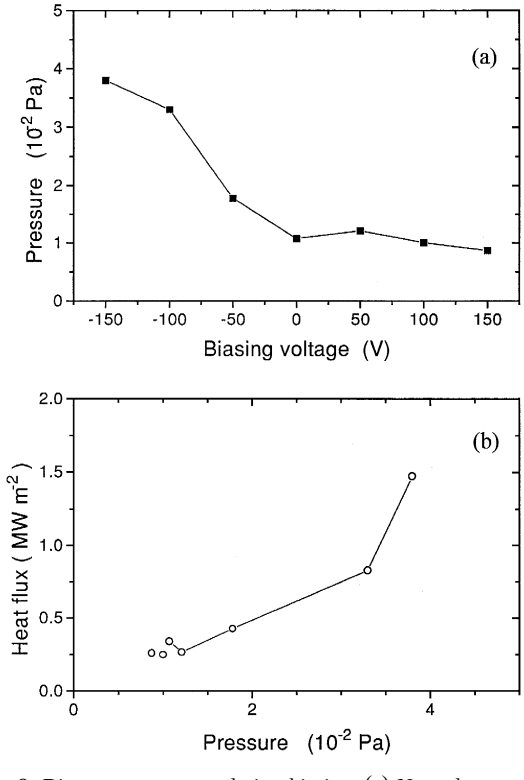

Fig. 8. Divertor parameters during biasing. (a) Neutral gas pressure versus biasing voltage. (b) Heat flux deposited on outer plates versus neutral pressure.

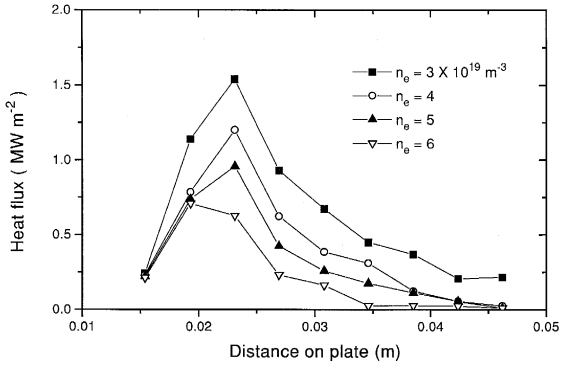

Fig. 9. Heat flux deposition on the outer divertor plates during negative biasing ($V_p = -150$ V), at different plasma densities.

the neutral pressure is not sufficient to counterbalance the increased heat flux to the divertor, the energy deposited on the divertor plates continuously increases with pressure, within the present pressure range (Fig. 8(b)). This increased heat load on the divertor plates during negative biasing has adverse effects on the plates. This problem would have to be solved in order to take full advantage of biasing.

To investigate detachment during biasing, a density scan has been performed. Fig. 9 shows the heat flux profile on the outer divertor plates at different plasma densities under negative divertor biasing with $V_b = -150$ V. The heat flux on the plates finally starts to drop at a high density around $\bar{n}_e = 6\text{–}7 \times 10^{19}$ m^{-3}. At such a high plasma density, the divertor neutral pressure (Fig. 10(a)) increases strongly to a value which is eight times higher than that in the unbiased case. At this higher pressure, the heat flux deposited on the divertor plates finally decreases as a function of pressure (Fig. 10(b)). From these observations, it is clear that the neutral gas pressure in the divertor region plays a key role in reducing energy deposition on the divertor plates. It is useful to puff gas directly in the divertor region to increase the local gas pressure and generate a gas cushion in front of the divertor plates. This will help to reduce the heat load on the divertor plates during negative divertor biasing.

4.3. Lower hybrid current drive and heating

Lower hybrid (LH) waves at 3.7 GHz have been used for current drive and plasma heating in TdeV. Up to 1.0 MW of LH power was launched using a multijunction antenna with refractive index $N_{\|}$ variable from 2.0 to 3.3 [16]. Fig. 11 shows the heat flux distributions on both outer and inner plates with LH current drive and heating (1.0 MW, $N_{\|} = 3.0$). For comparison, the heat flux distribution without RF is also shown as dashed lines. The arrows on the horizontal axis in the graph represent the locations of the magnetic separatrices predicted by the

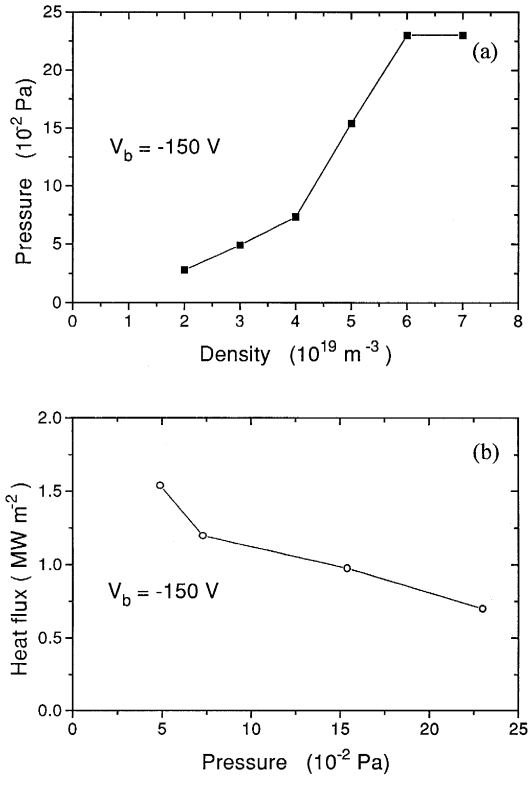

Fig. 10. With biasing voltage of -150 V, (a) divertor neutral pressure versus plasma density, (b) heat flux deposited on outer plates versus divertor pressure.

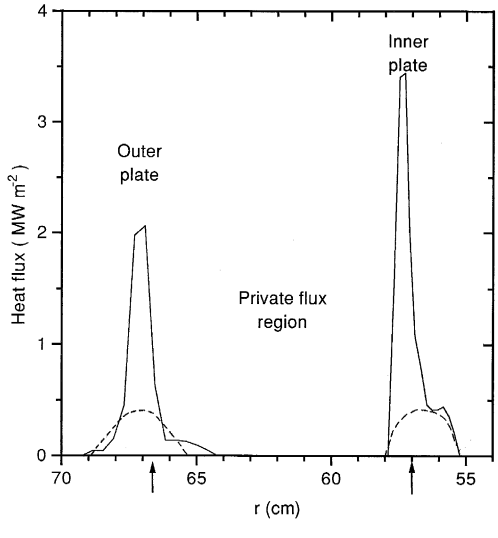

Fig. 11. Heat flux distribution on both outer and inner plates with (solid line) and without (dashed line) LH current drive/heating. The arrows on the *x*-axis indicate the magnetic separatrices predicted by the Lackner equilibrium code.

Lackner equilibrium code [29]. During normal ohmic heating discharges, the heat flux distribution on the plates is rather broad. In that case, to determine the exact magnetic separatrix from the heat flux distribution is not possible. However, during the LH phase, an intensified narrower heat flux distribution profile is formed on the divertor plates, especially on the inner divertor plates. This is caused by suprathermal electron bombardment of the divertor plate. The lower hybrid waves interact with the plasma electrons and generate a suprathermal electron tail. These electrons travel so fast along the open field lines in the vicinity of the magnetic separatrix that they hit the divertor plate before they can diffuse across the magnetic field lines. The preference for the inner plates by the suprathermal electrons in this case is simply due to the direction of the poloidal magnetic field with respect to the phase velocity of LH wave. This narrow bright band on the plate can be used to determine the location of the magnetic separatrix. The results compare well with predictions as shown in Fig. 11.

5. Conclusion

In summary, infrared imaging of the divertor plates in TdeV has been performed. The PDE/Protran finite element code was used to calculate the incident heat flux deposited on the divertor plates. For Ohmically heated discharges, the divertor plate temperature decreases with increasing plasma density, suggesting plasma detachment from the divertor plates at higher plasma densities (above 4.0×10^{19} m^{-3}). During divertor biasing experiments, the heat flux increases on the divertor plates as a result of the $\boldsymbol{E} \times \boldsymbol{B}$ flow. Higher plasma density is required to bring divertor temperature low enough for charge exchange to dominant over ionization. Along with the increase in density, the neutral pressure also increases. This process reduces the heat flux to the divertor plates. During the LH current drive/heating phase, the heat flux distribution on the plates becomes narrower and increases in intensity, resulting from fast suprathermal electron bombardment on the divertor plates. This can be used to determine the location of the magnetic separatrix, though it is definitely not desirable from the thermomechanical and erosion points of view (carbon 'blooming').

Acknowledgements

The authors are grateful to all members of the TdeV team; in particular, S. Ernst, Y. Drolet, F. Bourget, F. Brunet and F. Méo are acknowledged with gratitude for their technical assistance. The authors would also like to thank Drs B. Gregory, R. Décoste, B. Stansfield and W. Zuzak for their useful suggestions and advice. The Centre canadien de fusion magnétique is a joint venture of Hydro-Québec, Atomic Energy of Canada Ltd. and the Institut National de la Recherche Scientifique, in which MPB Technologies and Canatom Inc. also participate. It is principally funded by AECL, Hydro-Québec and INRS.

References

[1] T.W. Petrie et al., J. Nucl. Mater. 196–198 (1992) 848.
[2] I.H. Hutchinson et al., Phys. Plasmas 1 (1994) 1511.
[3] I.H. Hutchinson, Nucl. Fusion 34 (1994) 1337.
[4] B. Lipschultz et al., J. Nucl. Mater. 220–222 (1995) 50.
[5] T.W. Petrie et al., in: Proc. 18th. Europ. Conf. on Controlled Fusion and Plasma Physics, Berlin, Vol. 3 (1991) p. 237.
[6] P. Couture et al., Phys. Lett. A163 (1992) 204.
[7] R. Décoste et al., in: Plasma Physics and Controlled Nuclear Fusion Research 1992, Vol. 1 (IAEA, Vienna, 1993) p. 383.
[8] A.H. Sarkissian et al., Plasma Phys. Control. Fusion 35 (1993) 1175.
[9] B. Terreault et al., J. Nucl. Mater. 196–198 (1992) 226.
[10] B. Terreault et al., Nucl. Fusion 32 (1992) 1181.
[11] A. Boileau et al., Nucl. Fusion 32 (1992) 995.
[12] B.C. Gregory et al., in: Contributions to High-Temperature Plasma Physics, eds. K.H. Spatschek and J. Uhlenbusch (Akademie Verlag, Berlin, 1994) p. 34.
[13] D. Whyte et al., Nucl. Fusion 34 (1994) 203.
[14] A.H. Sarkissian et al., J. Nucl. Mater. 220–222 (1995) 223.
[15] J.L. Lachambre et al., in: Proc. 20th EPS Conf. on Controlled Fusion and Plasma Physics, Lisbon, Vol. 17C, Part II (European Physical Society, 1993) p. 4.
[16] Y. Demers et al., in: Proc. 21th EPS Conf. on Controlled Fusion and Plasma Physics, Montpellier, Vol. 18B, Part III (European Physical Society, 1994) p. 1086.
[17] J.P. Gunn et al., Rev. Sci. Instrum. 66 (1995) 154.
[18] J. Mailloux et al., Bull. Am. Phys. Soc. 39 (1994) 1534, Internal Report CCFM RI 451e.
[19] N. Richard et al., Bull. Am. Phys. Soc. 39 (1994) 1533, Internal Report CCFM RI 451e.
[20] M.S. Carslaw and J.C. Jaeger, Conduction of Heat in Solids (Oxford, Clarendon, 1959).
[21] D.N. Hill et al., Rev. Sci. Instrum. 59 (1988) 1878.
[22] A.V. Chankin et al., Plasma Phys. Control. Fusion 36 (1993) 403.
[23] G. Sewell, Analysis of a Finite Element Method: PDE/Protran (Springer, Berlin, 1985).
[24] G. Sewell, The Numerical Solution of Ordinary and Partial Differential Equations (Academic Press, New York, 1988).
[25] P.C. Stangeby, Nucl. Fusion 33 (1993) 1695.
[26] D. Michaud et al., J. Nucl. Mater. 196–198 (1992) 316.
[27] R.R. Weynants, Plasma Phys. Control. Fusion 37 (1995) 63.
[28] J.P. Gunn et al., Bull. Am. Phys. Soc. 39 (1995) 1712.
[29] K. Lackner, Comp. Phys. Commun. 12 (1976) 33.